

Ge n-channel FinFET with optimized gate stack and contacts

M.J.H. van Dal, B. Duriez, G. Vellianitis, G. Doornbos,
R. Oxland, M. Holland, A. Afzalian, Y.C. See, M. Passlack, C.H. Diaz¹

TSMC, Kapeldreef 75, B-3001 Leuven, Belgium, ¹TSMC R&D Hsinchu 300-75 Taiwan, email: mark_van_dal@tsmc.com

Abstract

Whilst high performance p-channel Ge MOSFETs have been demonstrated [1-4], Ge n-channel MOSFET drive current has been lagging behind mainly hampered by high access resistance and poor gate stack passivation [5-9]. In this work, we address these issues on a module level and demonstrate Ge enhancement mode nMOS FinFETs fabricated on 300mm Si wafers implementing optimized gate stack ($D_{it} < 2 \times 10^{11} \text{ eV}^{-1} \cdot \text{cm}^{-2}$), n^+ -doping ($N_d > 1 \times 10^{20} \text{ cm}^{-3}$) and metallization ($\rho_c = 1 \times 10^{-7} \Omega \text{cm}^2$) modules. $L_G \sim 40 \text{ nm}$ devices achieved $I_{on} = 50 \mu\text{A}/\mu\text{m}$ at $I_{off} = 100 \text{nA}/\mu\text{m}$, $S \sim 124 \text{ mV/dec}$, at $V_{DD} = 0.5 \text{ V}$. The same gate stack and contacts were deployed on planar devices for reference. Both FinFET and planar devices in this work achieved the highest reported g_m/S_{sat} at 0.5 V to date for Ge nMOS enhancement mode transistors to the best of our knowledge at shortest gate lengths.

Ge modules for NMOS

n-Ge doping - Using an n^+ /p junction with P implantation, activation and diffusion was studied for different annealing techniques. Secondary Ion Mass Spectrometry (SIMS) data after activation are shown in Fig. 1. Activation of P in Ge can be achieved at low temperature [10] but we find active doping concentration N_{act} to not exceed $1 \times 10^{19} \text{ cm}^{-3}$ irrespective of annealing time. As suggested in [11], this may be related to implantation damage-induced acceptor formation resulting in lower P activation. At medium temperature, P-vacancy clusters become mobile leading to a typical box-like profile and N_{act} of mid- 10^{19} cm^{-3} (Fig. 1). The optimized process achieves abrupt and high N_{act}

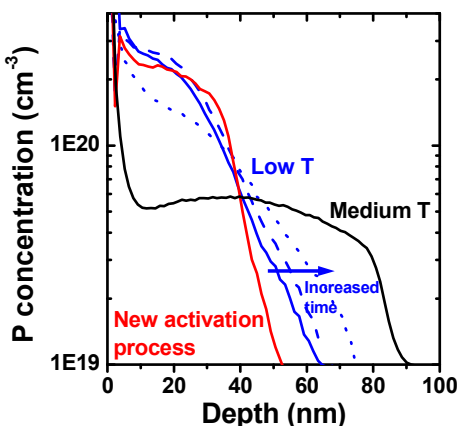


Figure 1: SIMS of phosphorus in Ge annealed using different annealing techniques. At low T we estimate $1 \times 10^{19} \text{ cm}^{-3}$ from R_s . The box-like profile at medium T is indicative of PV pair diffusion achieving N_{act} of mid- 10^{19} cm^{-3} . Our new activation process provides high N_{act} and junction abruptness of $\sim 4.5 \text{ nm/dec}$.

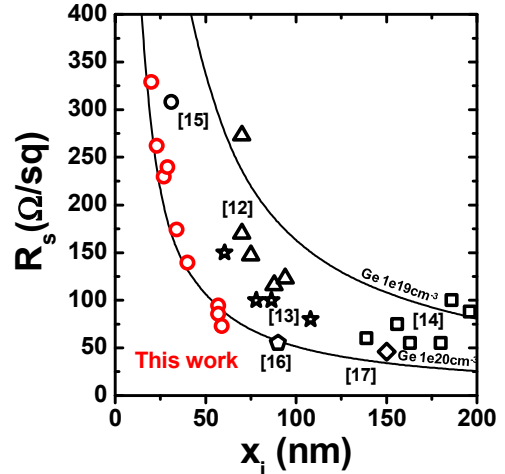


Figure 2: μ4PP R_s vs. x_j for optimized, scaled n-Ge junctions benchmarked with literature data [12-17]. Our data represent best R_s - x_j values to date following the $N_{act} = 1 \times 10^{20} \text{ cm}^{-3}$ trend line down to 23 nm junction depth.

junctions yielding the best R_s - x_j envelope reported to date for Ge n^+ /p junctions (Fig. 2) [12-17].

n-Ge metallization - As Me/Ge contacts show strong pinning close to the Ge valence band [18], high N_{act} at the metal/Ge interface is crucial to promote tunneling through the Schottky barrier and to achieve ohmic contacts. We investigated NiGe/n-Ge contacts by circular transmission line method (CTLM) structures. After implantation, anneal and patterning (248nm lithography), Ni was deposited and NiGe was formed. The unreacted Ni was removed by a selective wet etch. We developed a new CTLM contact resistivity (ρ_c) extraction model based on Reeves model [19] that captures the parasitic metal resistance R_{ME} contribution (*i.e.* NiGe sheet resistance). Fig. 3 shows extracted parameters. We found that for P-doped Ge, increased Ni thickness leads to

CTLM: spacing 0.35 – 32 μm

Doping species	Ni	ρ_c ($\Omega \cdot \text{cm}^2$)	R_{sc} (Ω/sq)	R_{me} (Ω/sq)
P	thin	5.0e-6	148	8.5
P	thick	8.8e-5	133	3.5
As	thin	1.1e-7	95	8.5
As	thick	1.9e-7	93	3.5
B	thin	5.4e-7	38	9

Figure 3: ρ_c and sheet resistance of n^+ Ge, R_{sc} determined from CTLM using new extraction model (not shown). NiGe sheet resistance, R_{me} , used as input parameter, is based on μ4PP measurements. Results for P are in line with [20]. The lowest ρ_c achieved was $1.1 \times 10^{-7} \Omega \text{cm}^2$.

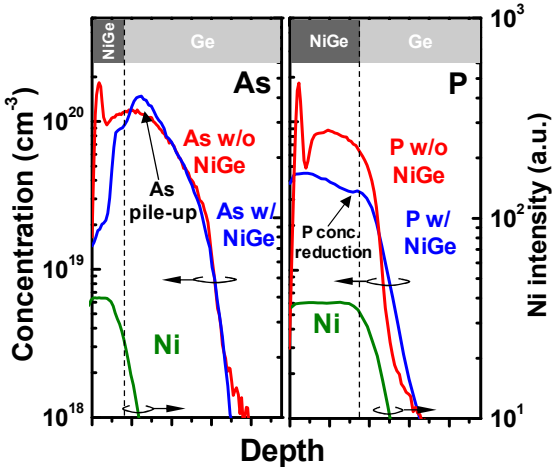


Figure 4: SIMS of As (left) and P (right) in Ge with or without NiGe formation. As piles up at the NiGe/Ge interface while the P concentration is reduced considerably.

higher ρ_c , while for As-doped Ge ρ_c remains low ($< 2 \times 10^{-7} \Omega\text{cm}^2$). The effect is largely due to higher dopant concentration at the NiGe/Ge interface as shown in Fig. 4. The lowest ρ_c achieved was $1.1 \times 10^{-7} \Omega\text{cm}^2$ which compares well with lowest values reported [20-23].

Ge gate stack - Interfacial treatments, high- κ optimization and treatments of the gate stacks reported in [3] were deployed in this work aiming for a device design with sub 1nm EOT scaling capability. Multi-frequency C-V for a $100 \times 100 \mu\text{m}^2$ MOSCAP with EOT = 1.3 nm is shown in Fig. 5. The small frequency dispersion in depletion to accumulation region is indicative of a low density of electrically active traps at and close to the dielectric/Ge interface. Low-T C-V analysis was used to extract D_{it} across the Ge band-gap (Fig. 6); the Hi-Lo method gave similar D_{it} ; there is no dependence on EOT (Fig. 7). $D_{it} \sim 2 \times 10^{11} \text{ eV}^{-1}\text{cm}^{-2}$ was found around mid-gap. The D_{it} levels achieved in this work are amongst the lowest reported on n-type Ge(100) and Ge(110) at scaled EOTs of 1-3 nm [24-25].

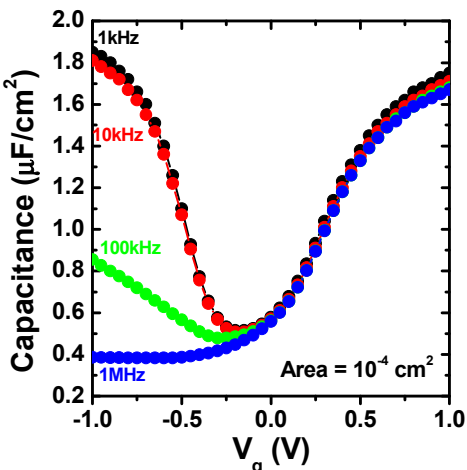


Figure 5: Multi-frequency C-V for a $100 \times 100 \mu\text{m}^2$ MOSCAP. The small frequency dispersion in depletion to accumulation region is indicative of a low density of electrically active traps at and close to the dielectric/Ge interface.

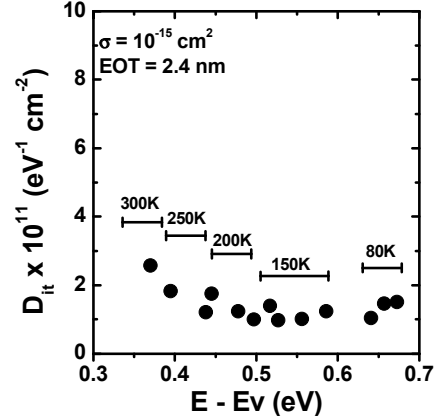


Figure 6: D_{it} vs. energy from conductance method at temperatures ranging from 80 to 300 K. D_{it} of $2 \times 10^{11} \text{ eV}^{-1}\text{cm}^{-2}$ was found around midgap.

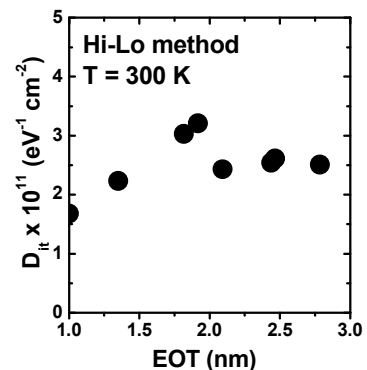


Figure 7: Midgap D_{it} dependence on EOT. D_{it} remains low at low EOT.

Ge enhancement mode NMOS Transistors

Enhancement mode n-channel Ge planar (001) FETs and (001)/(110) FinFETs were fabricated using Ge-in-STI 300 mm Si wafers as in [1, 2] and the device process including aspect-ratio trapping as described in [1-3], respectively. Gate-to-channel capacitance (for several CETs) and C-V curves (for the same CETs) for the planar MOSFETs are shown in Fig. 8. Effect of annealing conditions for contacts on device performance becomes

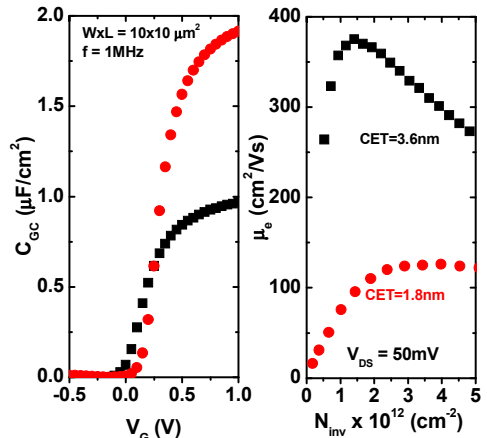


Figure 8: Gate-to-channel capacitance (for several CETs) and mobility curves (for the same CETs) for optimized gate dielectric (planar devices).

apparent from Figs. 9-11. Significant improvement in g_m (Fig. 9) and short channel effect (SCE) control (Fig. 10) is observed when optimized contacts are used. R_{ext} was extracted as $500 \Omega\mu\text{m}$ while for the reference devices $R_{ext} \sim 60 \text{k}\Omega\mu\text{m}$ was estimated (Fig. 11). Further SCE immunity is achieved implementing the FinFET architecture (Fig. 10). Fig. 12 shows g_m and S as a function of L_g for the FinFETs. Sub-threshold swing of 76mV/dec at $V_{ds} = 50 \text{ mV}$ and $L_g = 60 \text{ nm}$ is achieved. Transfer and output characteristics of the best short-channel device are shown in Figs. 13-14. Our nGe planar and FinFETs are benchmarked in Fig. 15 and exhibit highest g_m/S_{sat} at shortest gate length and scaled EOT compared to published results for enhancement mode Ge nFETs on (100) or (111) surfaces [6-9].

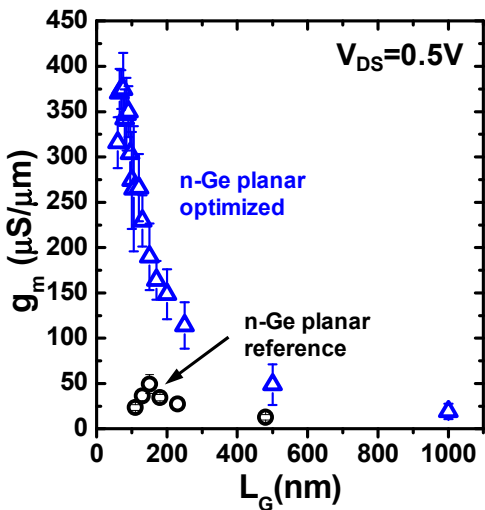


Figure 9: Peak- g_m at $V_{ds} = 0.5 \text{ V}$ as function of gate length for Ge n-channel planar FETs comparing reference and optimized devices.

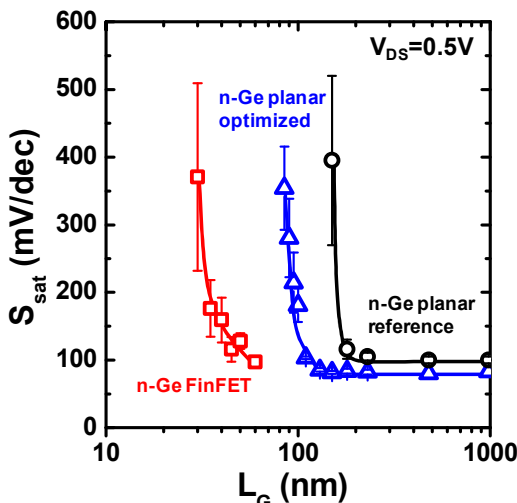


Fig. 10: Sub-threshold swing at $V_{ds} = 0.5 \text{ V}$ as a function of gate length for Ge n-channel planar FETs (reference and optimized) and FinFETs. Roll-up is improved when optimized contacts are implemented. FinFETs provide even better SCE control.

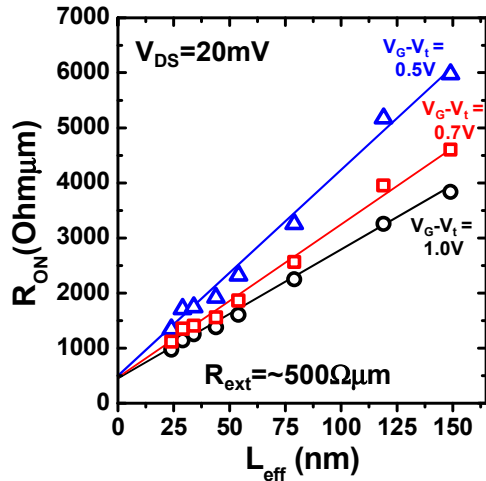


Figure 11: Average R_{on} ($\equiv V_{ds}/I_{ds}$ with $V_g - V_t = 0.5, 0.7, 1.0 \text{ V}$ and $V_{ds} = 20 \text{ mV}$) vs. effective gate length L_{eff} of Ge planar devices. R_{ext} was determined as $500 \Omega\mu\text{m}$. For comparison R_{ext} of reference devices is $\sim 60 \text{k}\Omega\mu\text{m}$.

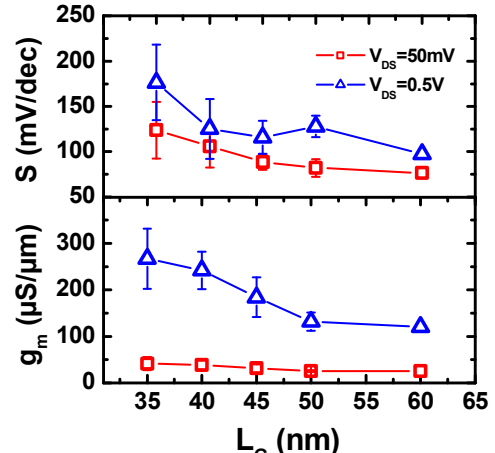


Figure 12: Sub-threshold swing and peak- g_m at $V_{ds} = 50 \text{ mV}, 0.5 \text{ V}$ as function of gate length for Ge n-channel FinFETs. At $L_g = 60 \text{ nm}$, $S = 78 \text{ mV/dec}$ at $V_{ds} = 50 \text{ mV}$.

Conclusions

We report Ge n-channel FinFETs implementing optimized gate stack ($D_{it} < 2 \times 10^{11} \text{ eV}^{-1}\text{cm}^{-2}$), n^+ -doping ($N_{\text{act}} > 1 \times 10^{20} \text{ cm}^{-3}$) and metallization ($\rho_c = 1 \times 10^{-7} \Omega\text{cm}^2$) modules. Both Ge nMOS FinFETs and planar transistors fabricated on (001) substrates in this work achieved the highest performance and g_m reported to date for Ge enhancement-mode NFETs with 0.5 V V_{DD} and $I_{off} < 100 \text{nA}/\mu\text{m}$ at the shortest gate-lengths ($\sim 40 \text{ nm}$ on Fin-FETs, $\sim 90 \text{ nm}$ on planar transistors) and lowest S_{sat} ($\sim 120 \text{ mV/dec}$) to the best of our knowledge with sub 1nm EOT scaling capability.

Acknowledgement - The authors thank IMEC for processing capabilities and technical support, and Dr. Y. C. Sun for management support.

References

- [1] M.J.H. van Dal *et al.*, *IEDM Tech. Dig.*, p. 521 (2012).
- [2] M.J.H. van Dal *et al.*, *IEEE Trans. Electron Devices* 61(2) p. 430 (2014).
- [3] B. Duriez *et al.* *IEDM Tech. Dig.*, p. 522 (2013).
- [4] J. Mitard *et al.*, *VLSI Symp. Proc.*, p. 138 (2014).
- [5] C.H. Lee *et al.*, *IEEE Trans. Electron Devices* 58(5) p. 1295 (2011).
- [6] C.T. Chung *et al.*, *IEDM Tech. Dig.*, p. 383 (2012).
- [7] S.-H. Hsu *et al.*, *IEDM Tech. Dig.*, p. 525 (2012).
- [8] W.B. Chen *et al.*, *IEDM Tech. Dig.*, p. 420 (2010).
- [9] H. Wu *et al.*, *VLSI Symp. Proc.*, p. 96 (2014).
- [10] R. Duffy *et al.*, *Appl. Phys. Lett.* 96, 231909 (2010).
- [11] J. Kim *et al.*, *Appl. Phys. Lett.* 98, 082112 (2011).
- [12] A. Satta *et al.*, *Appl. Phys. Lett.* 88, 162118 (2006).
- [13] C.O. Chui *et al.*, *Appl. Phys. Lett.* 87 091909 (2005).
- [14] M. Posselt *et al.*, *J. Vac. Sci. Technol. B* 26, 430 (2008).
- [15] G. Hellings, Ph.D. thesis K. University of Leuven (2012).
- [16] C. Wündisch *et al.*, *Appl. Phys. Lett.* 95, 252107 (2009).
- [17] J. Kim *et al.*, *Appl. Phys. Lett.* 101, 112107 (2012).
- [18] T. Nishimura *et al.*, *Appl. Phys. Lett.* 91 123123 (2007).
- [19] G.K. Reeves, *Solid-State Electronics* 23, p 487 (1980).
- [20] M. Shayesteh *et al.*, *IEEE Trans. Electron Devices* 60(7) p. 2178 (2013).
- [21] G. Thareja *et al.*, *IEDM Tech. Dig.*, p. 245, (2010).
- [22] A. Firrincieli *et al.*, *Appl. Phys. Lett.* 99, 242104 (2011).
- [23] P.P. Manik *et al.*, *Appl. Phys. Lett.* 101, 182105 (2012).
- [24] C.H. Lee *et al.*, *VLSI Symp. Proc.*, p. 145 (2014).
- [25] R. Zhang *et al.*, *IEEE Trans. Electron Devices* 60 p. 927 (2013).

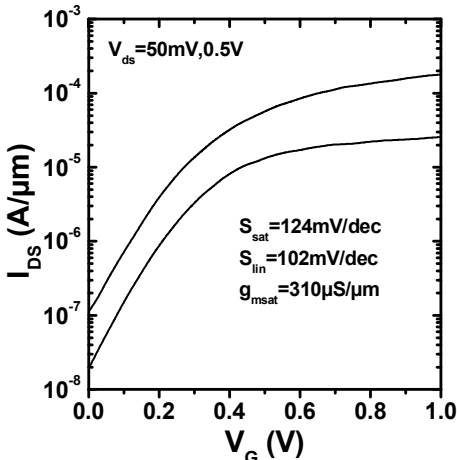


Figure 13: Linear and saturation ($V_{ds} = 50$ mV, 0.5 V) transfer characteristics of Ge n-channel FinFET ($L_G = 40$ nm). $I_{on} = 50 \mu\text{A}/\mu\text{m}$ at $I_{off} = 100 \text{nA}/\mu\text{m}$ ($V_{DD} = 0.5$ V)

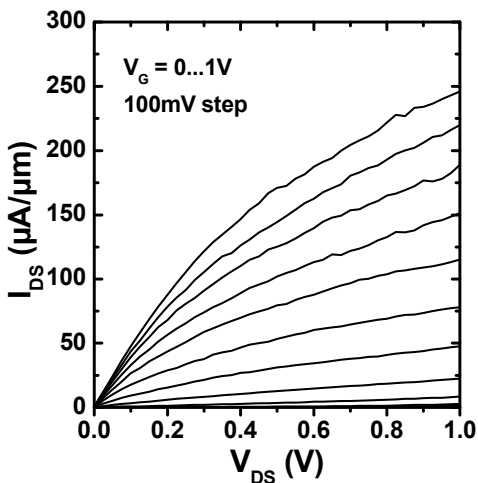


Figure 14: Output characteristics of Ge n-channel FinFET ($L_G = 40$ nm).

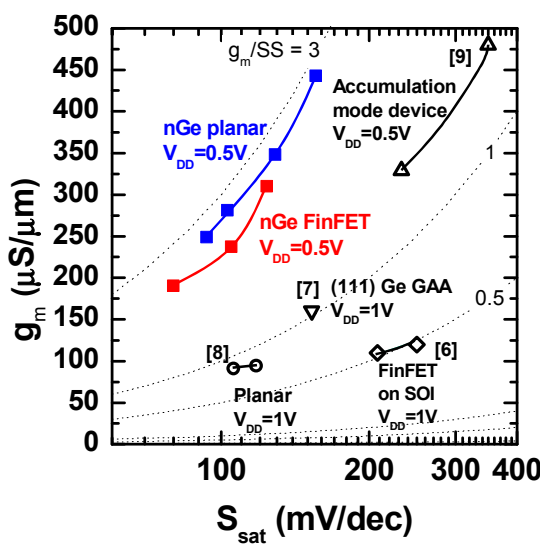


Figure 15: Extrinsic peak g_m vs. S_{sat} benchmark for Ge n-channel FETs [6-9], including our planar and FinFET data and accumulation mode nGe FET [9] at $V_{DD}=0.5$ V and FinFET on SOI [6], Gate-All-Around (GAA) with (111) Ge side walls [7] and planar Ge nFET [8] all at $V_{DD}=1$ V. Our data represent highest g_m/S for n-channel Ge FETs to date.